

## Supporting Information

### Photogeneration and the Bulk Quantum Efficiency of Organic Photovoltaics

Kan Ding<sup>1</sup>, Xiaoheng Huang<sup>2</sup>, Yongxi Li<sup>2</sup>, Stephen R. Forrest<sup>1,2,3</sup>

<sup>1</sup>*Department of Physics, University of Michigan*

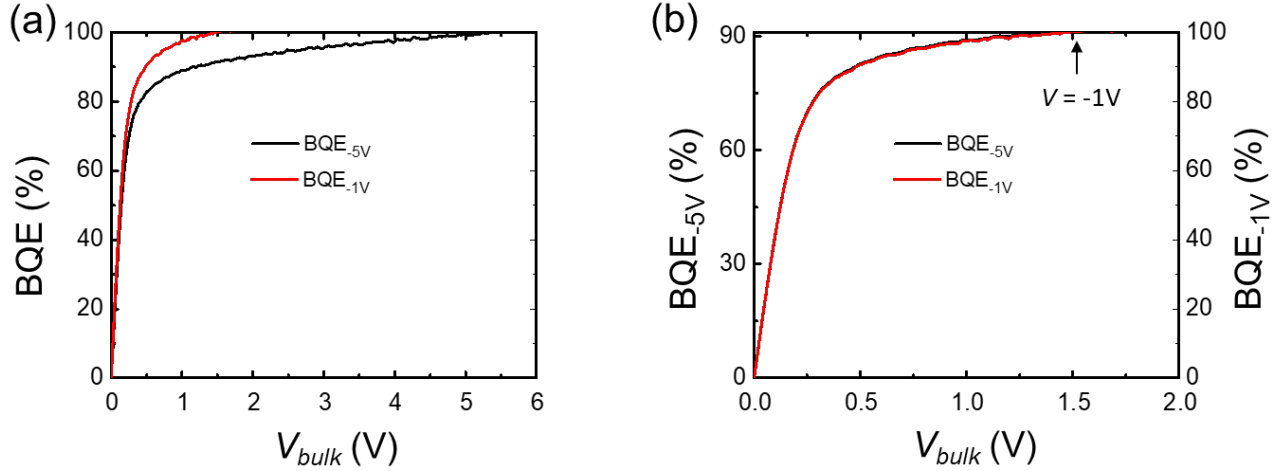
<sup>2</sup>*Department of Electrical Engineering and Computer Science, University of Michigan*

<sup>3</sup>*Departments of Material Science and Engineering, University of Michigan*

*Ann Arbor, MI 48109, USA*

#### The saturation current, $J_{\text{sat}}$

The BQE is calculated using  $J_{\text{ph}}$  ( $V = -1\text{V}$ ) as the saturation photocurrent,  $J_{\text{sat}}$ . However, to accurately calculate the BQE,  $J_{\text{sat}}$  should be at a reverse bias that is large enough such that BQE  $\rightarrow 1$  (see Eq. (3)). To test the effect of the choice of  $J_{\text{sat}}$ , we compare the BQE calculated using  $J_{\text{sat}} = J_{\text{ph}} (V = -1\text{V})$ , BQE<sub>-1V</sub>, with the BQE calculated using  $J_{\text{sat}} = J_{\text{ph}} (V = -5\text{V})$ , BQE<sub>-5V</sub>. Figure S1(a) shows the BQE(-1V) and BQE(-5V) vs.  $V_{\text{bulk}}$  for a PCE-10:BT-CIC OPV aged for 46 days. It can be seen that BQE(-1V) overestimates BQE by approximately 10% assuming BQE(-5V) is the actual BQE. However, BQE(-1V) and BQE(-5V) have the same dependence on  $V_{\text{bulk}}$  for  $V > -1\text{V}$ , as shown in Fig. S1(b). Therefore, although the absolute values of BQE can be slightly larger than their actual values, their relative changes vs.  $V_{\text{bulk}}$  are accurate. This overestimation of BQE is higher when the BQE is lower, resulting in an underestimation of  $\Delta\text{BQE}$ . Choosing  $J_{\text{sat}}$  to be at a larger reverse bias is preferred.

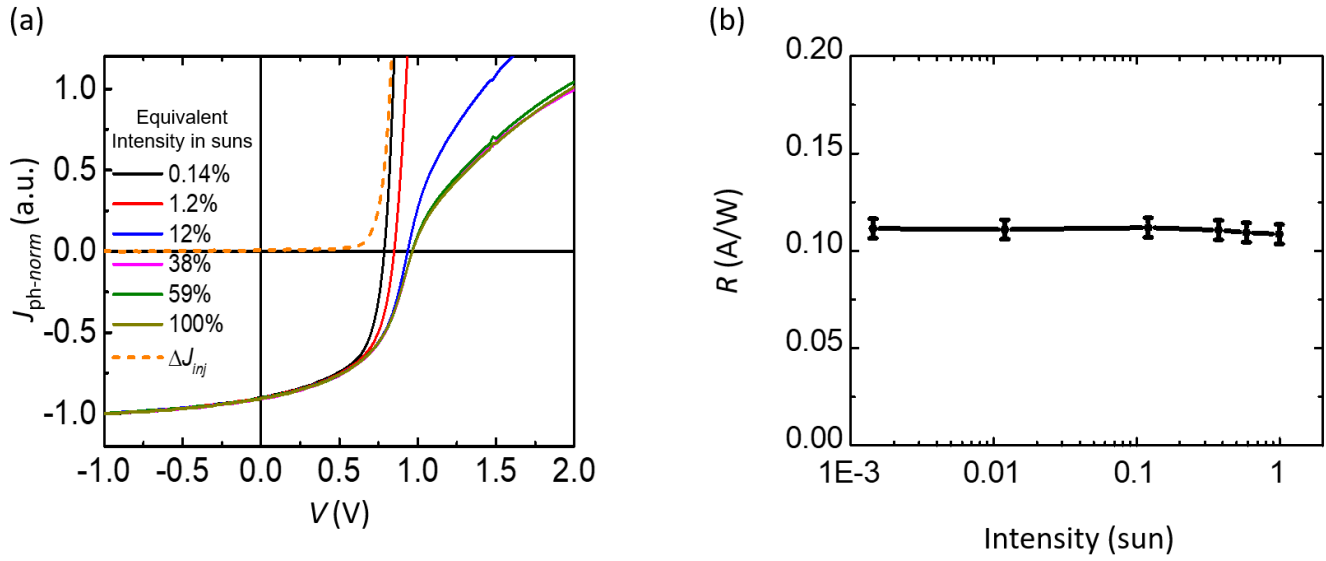


**Figure S1.** (a) BQE- $V_{bulk}$  characteristics of a PCE-10:BT-CIC OPV aged for 46 days using  $J_{sat} = J(-1V)$  and  $J_{sat} = J(-5V)$ . (b) BQE- $V_{bulk}$  characteristics in (a) plotted on different vertical scales.

### The intensity dependence of BQE

The BQE (as well as the  $r_{bulk}$  and  $r_{edge}$  in Eq. (1)) can have a light intensity dependence when multiparticle interactions are active. Figure S2 shows the  $J_{ph}$ - $V$  characteristics normalized to the  $J_{ph}(-1V)$  for a DBP:C<sub>70</sub> OPV at various white light illumination intensities. The shape of the  $J_{ph}$ - $V$  characteristics saturates when the intensity is  $> 0.38$  sun intensity, suggesting that the effects of higher-order mechanisms are negligible. This also makes BQE immune to errors related to the fluctuation in the light intensity during  $J$ - $V$  measurement. The different shapes of  $J_{ph}$  at low intensities are likely due to a calculation error when injection current ( $J_{inj}$ ) increases with light intensity due to photoconductivity.<sup>1</sup> As a result,  $J_{ph} = J - J_{dark}$  includes not only the photocurrent,  $J_{ph}$ , but also the increase in injection current,  $\Delta J_{inj}$ . This affects the shape of  $J_{ph}$ - $V$  characteristics at  $V > V_{oc}$  where  $J_{inj}$  is increasingly important. This increase in injected current is small and only causes a change of the  $J_{ph}$ - $V$  shape when the  $J_{ph}$  is also small. Assuming  $J_{ph-norm}(100\%)$  is the

normalized photocurrent, the increase of injected current at 0.14% sun is:  $\Delta J_{inj} = J_{ph-norm}(0.14\%) - J_{ph-norm}(100\%)$ , as shown by the dashed line in Fig. S2(a). Figure S2(b) shows the responsivity vs. light intensity of the OPV. The almost constant responsivity suggests that the low charge density approximation is valid, and multiparticle interactions are negligible.



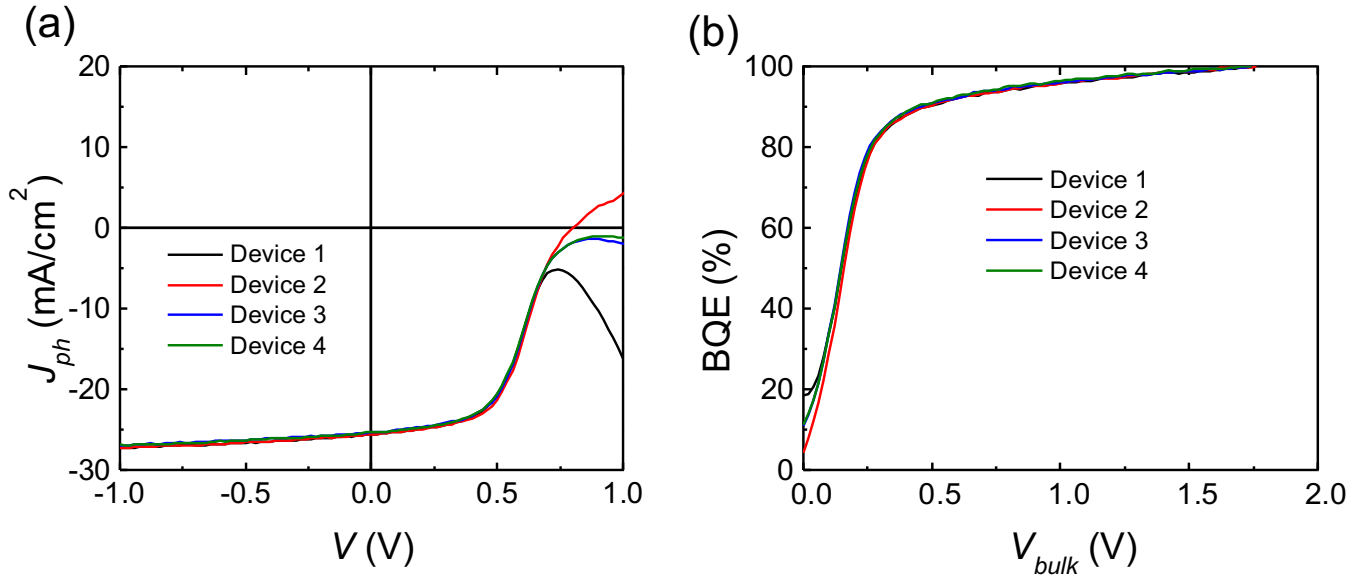
**Figure S2.** (a) Normalized photocurrent  $J_{ph}$  vs. voltage characteristics of a DBP:C<sub>70</sub> OPV under various illumination intensities, and the increase in injection current,  $\Delta J_{inj}$ . (b) The responsivity vs. light intensity.

### Errors in BQE due to fluctuations in contact resistance

Although BQE is not dependent on  $J_{dark}$ , the calculation of  $J_{ph}$  relies on the value of  $J_{dark}$ . When the contact is unstable (e.g., if Al contact is oxidized or the probes are not in solid contact with the electrodes), the  $J_{inj}$  under illumination may not equal  $J_{dark}$  even at light intensities comparable to 1 sun, causing an error in  $J_{ph}$  near the  $V_{bulk} = 0$  where  $J_{dark} \approx J_{ph}$ . Figure S3(a) shows the  $J_{ph}$ - $V$  characteristics of four identical PCE-10:BTCIC OPVs on the same substrate but with

different contact conditions. Due to poor contact, the shapes of the  $J_{ph}$  near the  $V_{bulk} = 0$  differ, causing an error in determining the  $V_{off}$ . In Fig. S3(b), the BQE- $V_{bulk}$  characteristics of the four devices are aligned by the linear sections on the rising edges to correct the error caused by the poor contacts. As a result, the BQE- $V_{bulk}$  curves after correction may not cross the origin.

**Figure S3.** (a)  $J_{ph}$ - $V$  characteristics of four identical PCE-10:BT-CIC OPVs on the same substrate



with various contact conditions. (b) Corrected BQE- $V_{bulk}$  characteristics of devices in (a).

### BQE Calculation

To get BQE- $V_{bulk}$  characteristics as well as  $J_{sat}$  and  $V_{off}$  for an OPV, the  $J$ - $V$  characteristics in the dark,  $J_D(V)$ , and under illumination,  $J(V)$ , are needed. The BQE- $V_{bulk}$  characteristics can be achieved as follows:

1. Calculate the photocurrent:  $J_{ph}(V) = J(V) - J_D(V)$ ;
2. Determine  $J_{sat}$  which is the value of  $J_{ph}$  at a certain reverse bias. It is recommendable to choose a large reverse bias as discussed above;

3. Determine  $V_{off}$  which is the value of  $V$  where  $J_{ph} = 0$ ;
4. Calculate BQE- $V_{bulk}$  characteristics:

$$\text{BQE}(V_{bulk}) = \frac{J_{ph}(V_{off} - V_{bulk})}{J_{sat}}$$

In the case of a poor contact as discussed above, the BQE- $V_{bulk}$  curve near  $V_{bulk}=0$  can be distorted, leading to a randomness in  $V_{off}$ . Figure S4(a) shows  $J_{ph}$ - $V$  characteristics of the same device with solid and poor contact. As a result,  $V_{off}$  of the poor contact curve is larger. To correct for this error, we recommend extending the linear section on the rising edge of the BQE- $V_{bulk}$  curve as shown in

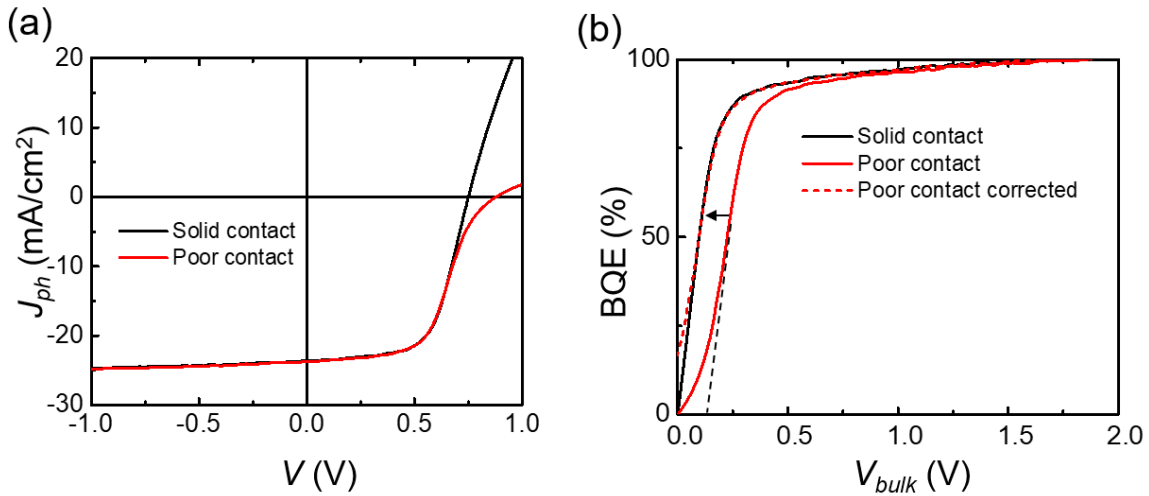
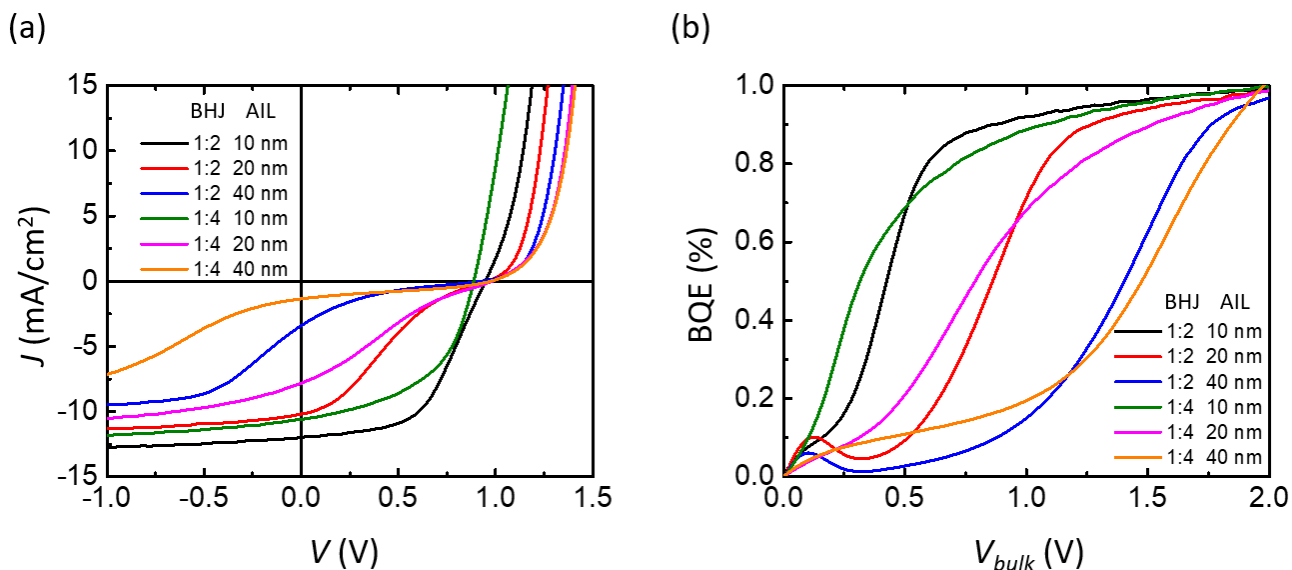


Fig. S4(b) and adjust the BQE- $V_{bulk}$  curve horizontally as well as the  $V_{off}$  value so that the extended line crosses the origin.

**Figure S4.** (a)  $J_{ph}$ - $V$  characteristics of a PCE-10:BT-CIC OPV with solid and poor contact. (b) As-calculated BQE- $V_{bulk}$  characteristics for solid and poor contact devices and corrected BQE- $V_{bulk}$  characteristics for the poor contact device.

## OPVs with Energy Barriers

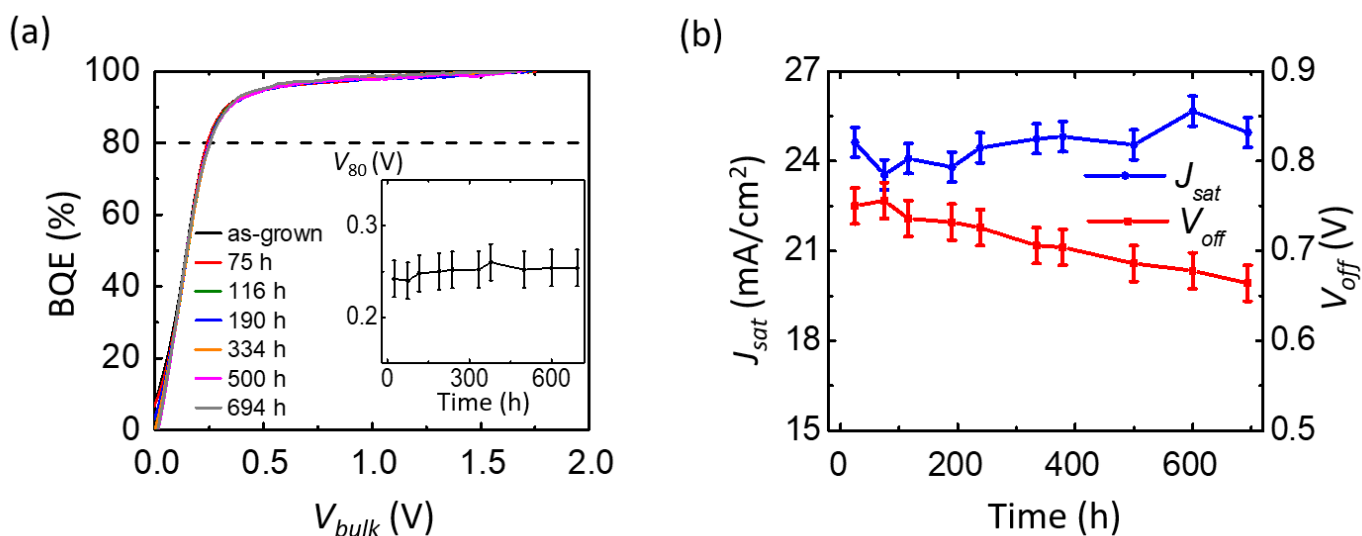
In previous work, we showed that in DBP:C<sub>70</sub> OPVs, a thin layer of C<sub>70</sub> acceptor interface layer (AIL) inserted between the BHJ and the anode buffer layer reduces the energy loss at the BHJ/anode buffer interface and hole collection is achieved by tunneling through the AIL. However, when the AIL thickness surpasses the hole tunneling distance, the AIL introduces an energy barrier and becomes a hole blocking layer, leading to a S-shaped  $J$ - $V$  characteristic.<sup>2</sup> This S-shape has been suggested to be due to the accumulation of photogenerated charges at the energy barrier.<sup>3</sup> Figure S5(a) shows the  $J$ - $V$  characteristics of DBP:C<sub>70</sub> OPVs with various mixing ratios and C<sub>70</sub> AILs with various thicknesses and the as-calculated BQE- $V_{bulk}$  characteristics are shown in Fig. S5(b). As a result of the energy barrier for holes between the AIL and the BHJ, the calculated BQs also become S-shaped and no longer represent the charge collection properties of the BHJs.



**Figure S5.** (a)  $J$ - $V$  characteristics of DBP:C<sub>70</sub> OPVs with various mixing ratios and C<sub>70</sub> AILs of various thicknesses. (b) As-calculated BQE- $V_{bulk}$  characteristics for OPVs in (a).

## Thermal Degradation of the Edges

To study the degradation of OPVs due to thermal effects, we heat the PCE-10:BT-CIC OPV on a hotplate in the dark at 45 °C. The device structure is: ITO 150nm/ZnO 30 nm/IC-SAM/PCE-10:BT-CIC, 1:1.5, 80 nm/MoO<sub>x</sub> 10 nm/Al 100 nm. The BQE- $V_{bulk}$  characteristics vs. treatment time are shown in Fig. S6(a), and the  $V_{80}$  vs. time is shown in the inset. Figure. S6(b) shows the  $V_{off}$  and  $J_{sat}$  vs. time.

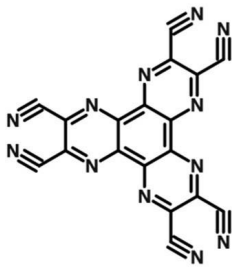

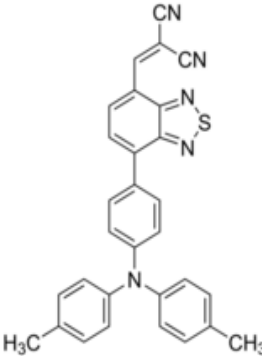
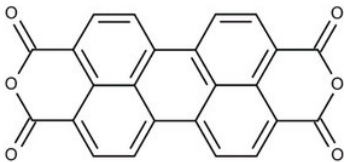
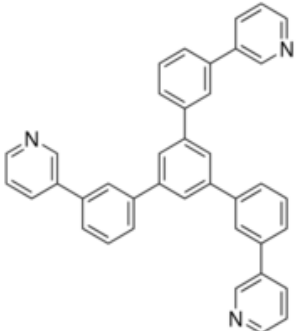


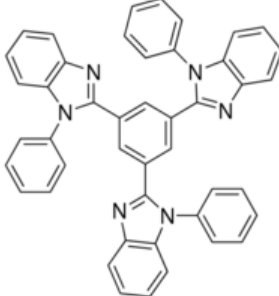
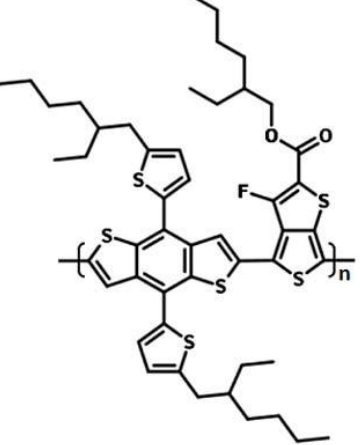
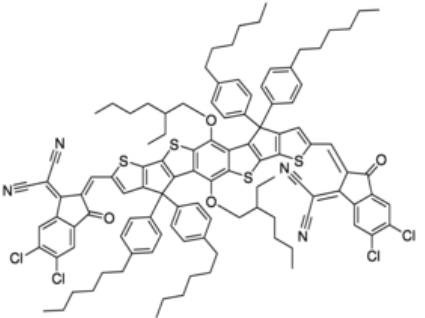
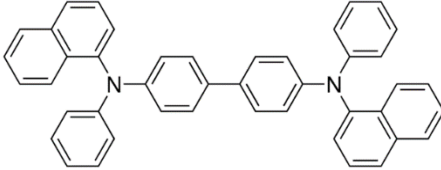
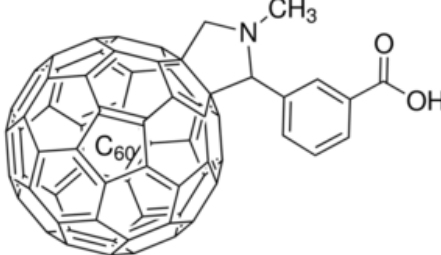
**Figure S6.** (a) BQE- $V_{bulk}$  characteristics of a PCE-10:BT-CIC OPV baked in dark at 45 °C. Inset:  $V_{80}$  vs. baking time. (b)  $V_{off}$  and  $J_{sat}$  vs. baking time.

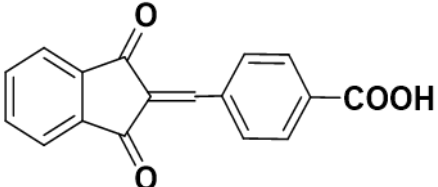
**Table S1.** Chemical names, structures and frontier orbital energies of molecules used.

Short Name	Full Chemical Name	Chemical structure	Frontier Orbital Energies
DBP	5,10,15,20-Tetraphenylbisbenz[5,6]indeno[1,2,3-cd:1',2',3'-lm]perylene		HOMO: 5.5 eV LUMO: 3.5 eV
C <sub>70</sub>	[5,6]-Fullerene-C70		HOMO: 6.2 eV LUMO: 4.0 eV
BPhen	Bathophenanthroline		HOMO: 6.4 eV LUMO: 3.0 eV
PEDOT: PSS	Poly(3,4-ethylenedioxythiophene)-poly(styrenesulfonate)		HOMO: 5.2 eV LUMO: 3.5 eV



HAT-CN	1,4,5,8,9,11-Hexaazatriphenylenehexacarbonitrile		HOMO: 7.5 eV LUMO: 4.4 eV
C <sub>60</sub>	Fullerene-C <sub>60</sub>		HOMO: 6.1 eV LUMO: 4.5 eV
DTDCPB	2-[(7-{4-[N,N-Bis(4-methylphenyl)amino]phenyl}-2,1,3-benzothiadiazol-4-yl)methylene]propanedinitrile		HOMO: 5.4 eV LUMO: 3.5 eV
PTCDA	Perylene-3,4,9,10-tetracarboxylic dianhydride		HOMO: 6.8 eV LUMO: 4.7 eV
TmPyPB	1,3,5-Tri(m-pyridin-3-ylphenyl)benzene, 1,3,5-Tris(3-pyridyl-3-phenyl)benzene		HOMO: 6.7 eV LUMO: 2.7 eV

TPBi	2,2',2''-(1,3,5-Benzinetriyl)-tris(1-phenyl-1- <i>H</i> -benzimidazole)		HOMO: 6.2 eV LUMO: 2.7 eV
PCE-10	Poly[4,8-bis(5-(2-ethylhexyl)thiophen-2-yl)benzo[1,2-b;4,5-b']dithiophene-2,6-diyl-alt-(4-(2-ethylhexyl)-3-fluorothieno[3,4-b]thiophene-)-2-carboxylate-2-6-diyl]]		HOMO: 5.2 eV LUMO: 3.7 eV
BTCIC	4,4,10,10-tetrakis(4-hexylphenyl)-5,11-(2-ethylhexyloxy)-4,10-dihydrodithienyl[1,2- <i>b</i> :4,5 <i>b'</i> ]benzodithiophene-2,8-diylbis(2-(3-oxo-2,3-dihydroinden-5,6-dichloro-1-ylidene)malononitrile)		HOMO: 5.5 eV LUMO: 4.1 eV
NPD	<i>N,N'</i> -Di(1-naphthyl)- <i>N,N'</i> -diphenyl-(1,1'-biphenyl)-4,4'-diamine		HOMO: 5.5 eV LUMO: 2.4 eV
C <sub>60</sub> -SAM	4-(1',5'-Dihydro-1'-methyl-2'H-[5,6]fullereno-C <sub>60</sub> -I <sub>h</sub> -[1,9-c]pyrrol-2'-yl)benzoic acid		

IC-SAM	4-((1,3-dioxo-1,3-dihydro-2H-inden-2-ylidene)methyl)benzoic acid	 <p>The image shows the chemical structure of 4-((1,3-dioxo-1,3-dihydro-2H-inden-2-ylidene)methyl)benzoic acid. It consists of a 1,3-dioxo-1,3-dihydro-2H-inden-2-ylidene group (a benzene ring fused to a five-membered ring with two carbonyl groups) connected via a double bond to a para-substituted benzene ring. The para-substituted benzene ring has a carboxylic acid group (-COOH) at the 4-position.</p>	
--------	--	--	--

**Table S2.** Parameters for fits in Fig. 5c.

Aging Time (hours)	$P_{trap}$	$C_{esc}$	$V_{esc}$ (V)
5	0.03	0.1	0.32
48	0.07	0.2	0.33
120	0.12	0.4	0.43
336	0.19	0.8	0.50
696	0.39	1.34	0.50
1056	0.44	1.1	0.61

**Table S3.** Parameters for fits in Fig. 7c.

Aging Time (hours)	$P_{trap}$	$C_{esc}$	$V_{esc}$ (V)
14	0.35	0.09	0.11
48	0.4	0.05	0.11
108	0.65	0.22	0.20
349	0.75	0.25	0.23
721	1.1	0.61	0.28
1095	1.2	0.70	0.29

## Reference

1. Renshaw, C. K.; Zimmerman, J. D.; Lassiter, B. E.; Forrest, S. R., Photoconductivity in donor-acceptor heterojunction organic photovoltaics. *Phys. Rev. B* **2012**, *86* (8), 085324.
2. Ding, K.; Forrest, S. R., Reducing Energy Losses at the Organic--anode-buffer Interface of Organic Photovoltaics. *Phys. Rev. Appl.* **2020**, *13* (5), 054046.
3. Sundqvist, A.; Sandberg, O. J.; Nyman, M.; Smått, J.-H.; Österbacka, R., Origin of the S-Shaped JV Curve and the Light-Soaking Issue in Inverted Organic Solar Cells. *Adv. Energy Mater.* **2016**, *6* (6), 1502265.